Supporting information

Sb-doped high-voltage $LiCoO_2$ enabled improved structural stability and rate capability for high-performance Li-ion batteries

Cong Chen [ab], Tianyu Li [a], Xiaofei Yang [a], Chao Qu [a], Yang Luo [ab], Yuxiao Wang [ab], Huamin Zhang [a], Hongzhang Zhang *[a] and Xianfeng Li *[a]

[a] Division of Energy Storage, Dalian National Laboratory for Clean Energy, Dalian Institute of Chemical Physics, Chinese Academy of Sciences, Zhongshan Road 457, Dalian, 116023, China. E-mail: zhanghz@dicp.ac.cn, lixianfeng@dicp.ac.cn
[b] University of Chinese Academy of Sciences, Beijing, 100049, China

Experiments section

In this study, bare $LiCoO_2$ and $LiCo_{1-x}Sb_xO_2$ (x=0.005, 0.01, 0.015 and 0.02) were synthesized by an simple high-temperature solid-phase method. The bare $LiCoO_2$ and $LiCo_{1-x}Sb_xO_2$ were prepared by using reagent-grade Li_2CO_3, Co_3O_4, Sb_2O_3 as precursors, the raw materials were sufficiently ground in an agate mortar and the mixed powders were sintered at 1000 °C for 10 h in air to obtain the intermediate products. Then, the intermediate products were ground again in an agate mortar and sintered for a second time at 900 °C for 10 h to obtain the final products. To compensate for the loss of lithium during the high-temperature process, 5 wt% excess Li_2CO_3 was added during the calcination. The reaction equation of the synthesis process is as the formula. The samples obtained can be used directly without subsequent processing.

$$6\ Li_2CO_3 + 4(1-x)\ Co_3O_4 + 6x\ Sb_2O_3 + (1-x)\ O_2 \rightarrow 12\ LiCo_{(1-x)}Sb_xO_2 + 6\ CO_2$$

The morphology and elements distribution of the obtained materials were investigated by scanning electron microscopy (SEM, JSM-7800F) attached with energy dispersive spectrometer (EDS) mapping. The powder X-ray diffraction (XRD, DX-2700) and in situ XRD were used to study the crystal structure of all synthetic materials, it equipping with Cu-Ka radiation (λ=0.154 nm) operated at 40 kV and 40 mA. The XRD dates were obtained from 10° to 90° in 2θ at a scanning rate of 10° min^{-1}. Transmission electron microscopy (TEM, JEM-2100) was used to identify the structure of the prepared samples. The particle sizes were analyzed by Malvern micron laser particle size analyzer (Mastersizer 2000).

The electrochemical behavior of as-prepared cathode materials was investigated in CR2016-type coin cells. The active materials were mixed with carbon black (Super P) and polyvinylidene difluoride (PVDF) (weight rate 8:1:1) in N-methyl pyrrolidone (NMP). The slurry was cast on an aluminum foil and directly dried in a vacuum oven at 80 °C overnight. The positive electrodes were cut into circular pieces with a diameter of 14 mm. The loading density was about 2.0±0.2 mg cm^{-2}. Cathodes were dried in a vacuum oven at 80 °C for 4h before assembling cells. The coin cells were assembled in an argon-filled glove box. The water vapor and oxygen concentration in the glove box were both less than 1 ppm. The lithium metal foil was as the counter electrode and the double-sided coated ceramic diaphragm was as the separator. The electrolyte used was TC-E9201-B purchased from Tinci Materials Technology. Galvanostatic charge-discharge test was performed using LAND battery test system (Wuhan, China) with voltages arranged from 3.0- 4.5 V. To investigate the cycling performance of bare $LiCoO_2$ and $LiCo_{1-x}Sb_xO_2$, the cells were cycled at 1 C (1 C=220 mA g^{-1}). The rate capacity of the cells was studied by charging at 1 C and discharging at different rates. Cyclic voltammetry (CV) measurements were performed on a CHI electrochemical

workstation with a scan rate of 0.1 mV s^{-1} in the voltage range of 3.0-4.5 V. The electrochemical impedance spectra (EIS) was performed on Solartron (SI 1287) electrochemical workstation with a frequency range from 1000 kHz to 0.01 Hz. All of the cells were tested at room temperature.

All calculations in this work were performed using the Vienna Ab initio Simulation Package (VASP)[1], within the framework of density functional theory (DFT). All calculations were based on the generalized gradient approximation (GGA)[2]method with Perdew-Burke-Ernzerhof (PBE)[3] functional for electronic exchange-correlation term. Van der Waals interaction was taken into account at DFT-D3[4, 5] with Becke-Jonson (BJ)[6] damping. The plane-wave basis set with a 520 eV cut off energy was employed to describe the states of valence electrons while the core electrons were treated with the projector augmented wave (PAW)[7] pseudopotentials. The calculated equilibrium lattice constant of $LiCoO_2$ is a=b=2.855 Å, c=13.974 Å, α=β=90, γ=120.

A p(4×4×1) supercell of $LiCoO_2$ and $LiCoSbO_2$ were constructed to model each system, which was $Li_{48}Co_{48}O_{96}$ and $Li_{48}Co_{47}SbO_{96}$ for each structure. 25%, 50%, and 75% of Li atoms were removed from the supercell respectively, to represent the delithiation structure of 25%, 50%, and 75%. The Brillouin zone integration was carried out with 3×3×3 Gamma point. The convergence thresholds for energy were set as 10^{-5} eV during ion relaxation, and the convergence thresholds for force were set as 0.05 eV·$Å^{-1}$. To model Li diffusion in $LiCoO_2$ and $LiCoSbO_2$, a p(2×2×1) supercell was built and the climbing-image nudged elastic band (CI-NEB) method with 4 images including DFT-D3(BJ) damping was applied and each transition state was confirmed to have a single imaginary vibrational frequency along with the reaction coordinate. The convergence thresholds for energy were set as 10^{-6} eV and the convergence thresholds for force were set as 0.05 eV·$Å^{-1}$ in the CI-NEB procedure.

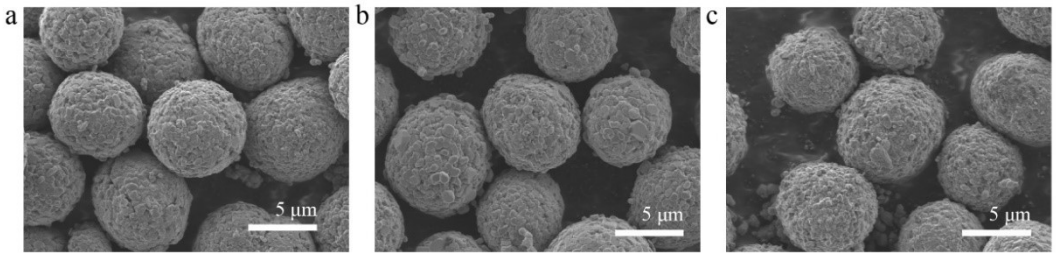

Fig. S1. Scanning electron microscopy (SEM) images of (a) $LiCo_{0.995}Sb_{0.005}O_2$, (b) $LiCo_{0.99}Sb_{0.01}O_2$, (c) $LiCo_{0.985}Sb_{0.015}O_2$.

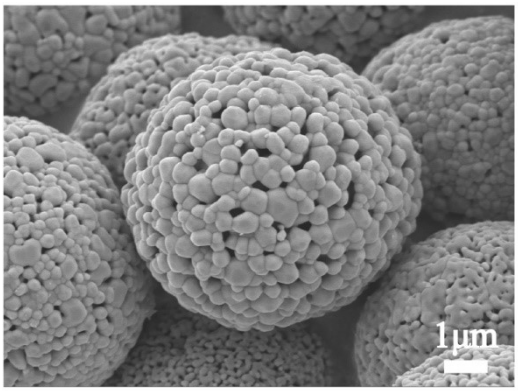

Fig. S2. Scanning electron microscopy (SEM) images of Co_3O_4.

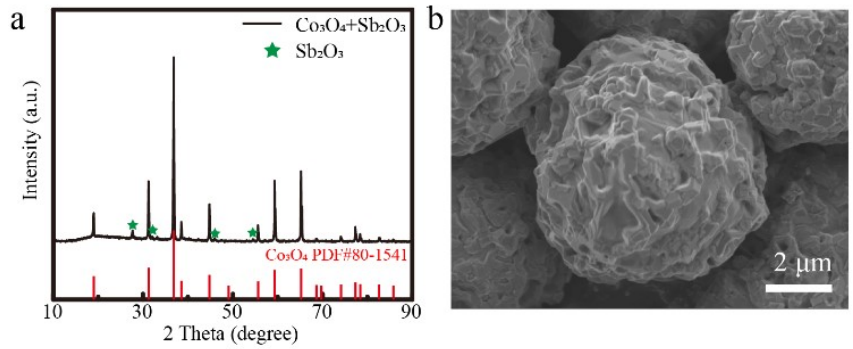

Fig. S3. (a) XRD pattern of Co_3O_4 and Sb_2O_3 after sintering, (b) SEM images of Co_3O_4 and Sb_2O_3 after sintering. The mixture of Co_3O_4 and Sb_2O_3 was sintered at 1000℃ for 10 h, and then sintered at 900℃ for 10 h.

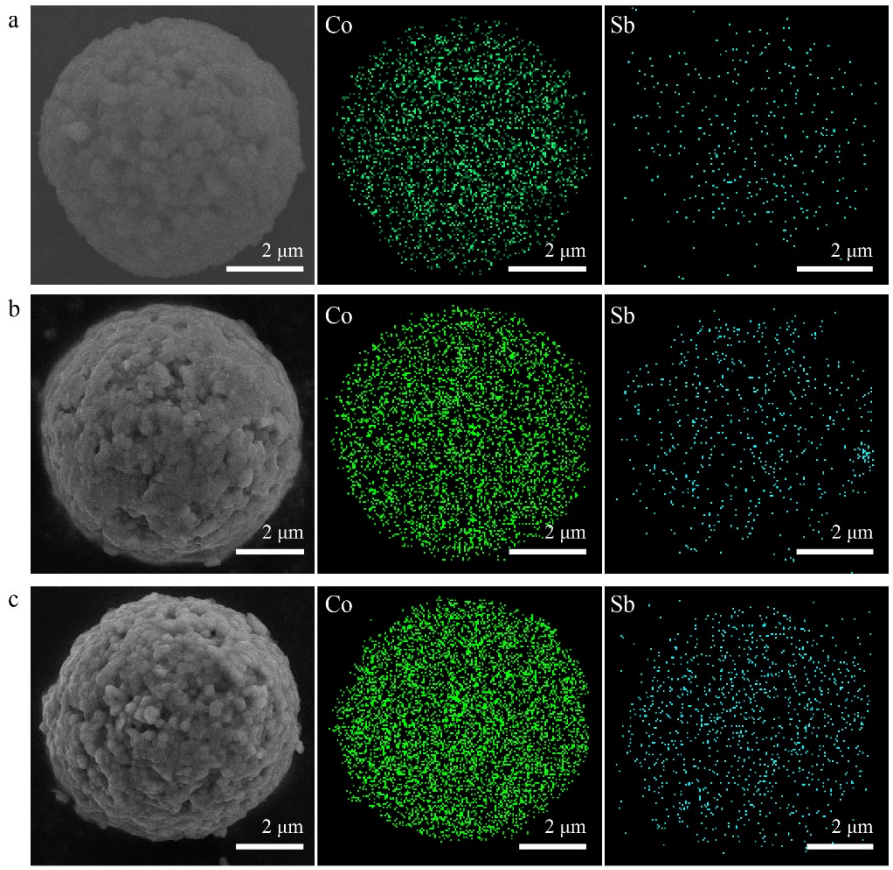

Fig. S4. EDS elemental mapping of Co and Sb in (a) $LiCo_{0.995}Sb_{0.005}O_2$ (b) $LiCo_{0.99}Sb_{0.01}O_2$ and (c) $LiCo_{0.985}Sb_{0.015}O_2$ samples.

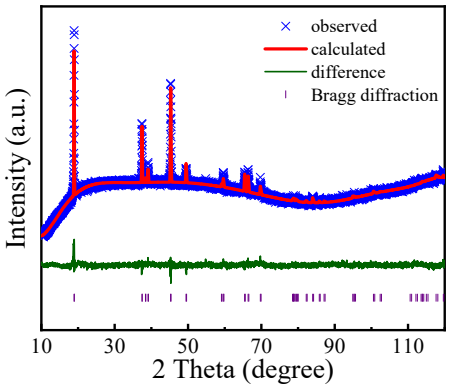

Fig. S5. Rietveld-refined XRD patterns of $LiCo_{0.98}Sb_{0.02}O_2$.

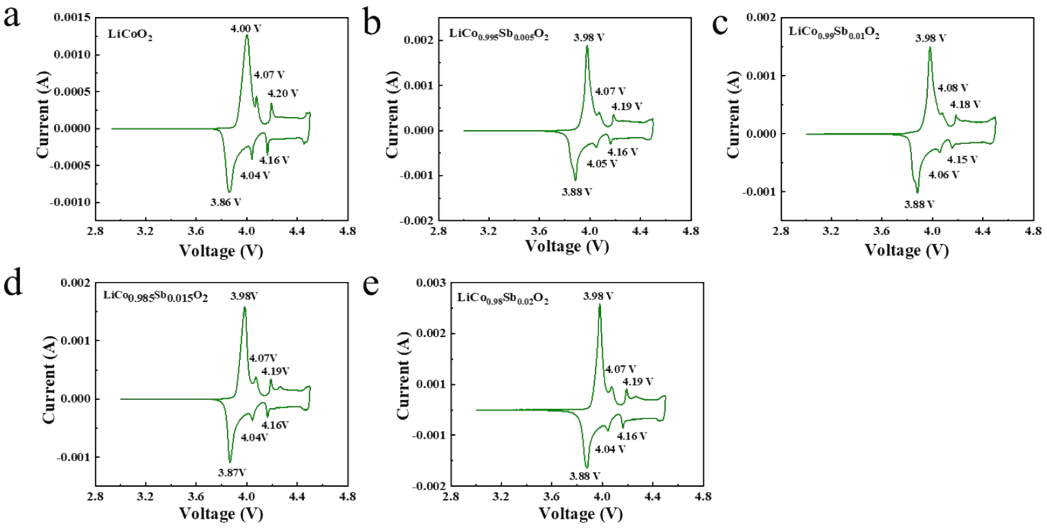

Fig. S6. Cyclic voltammogram curves of (a) $LiCoO_2$, (b) $LiCo_{0.995}Sb_{0.005}O_2$, (c) $LiCo_{0.99}Sb_{0.01}O_2$, (d) $LiCo_{0.985}Sb_{0.015}O_2$, (e) $LiCo_{0.98}Sb_{0.02}O_2$ in the voltage range of 3.0-4.5V with a scan rate of 0.1mV s^{-1}.

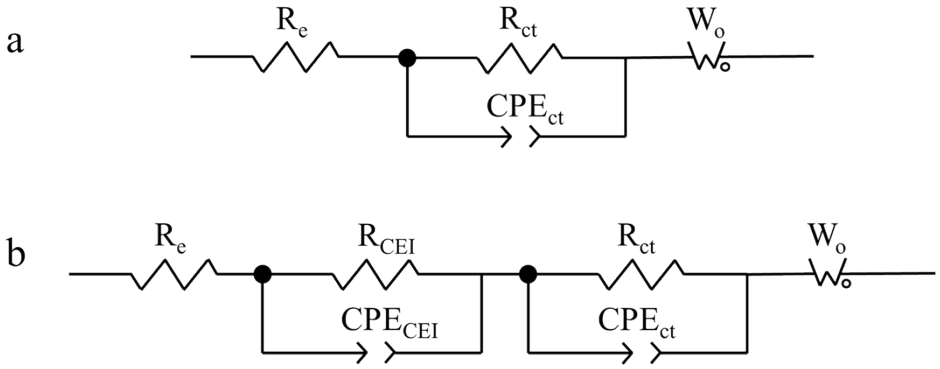

Fig. S7. The equivalent circuit models used for the fitting of EIS data. (a) pristine state before cycling and (b) after 100 cycles.

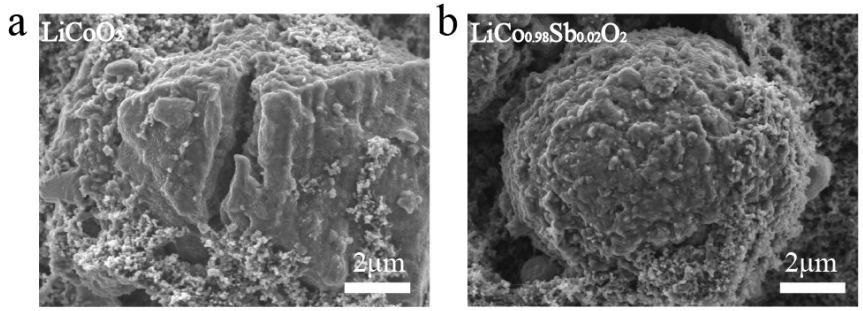

Fig. S8. Morphology of (a) $LiCoO_2$ and (b) $LiCo_{0.98}Sb_{0.02}O_2$ electrodes after cycling. It can be seen that the $LiCoO_2$ particles are cracked after cycling, while the $LiCo_{0.98}Sb_{0.02}O_2$ particles remain intact, so the introduction of Sb can improve the structural stability.

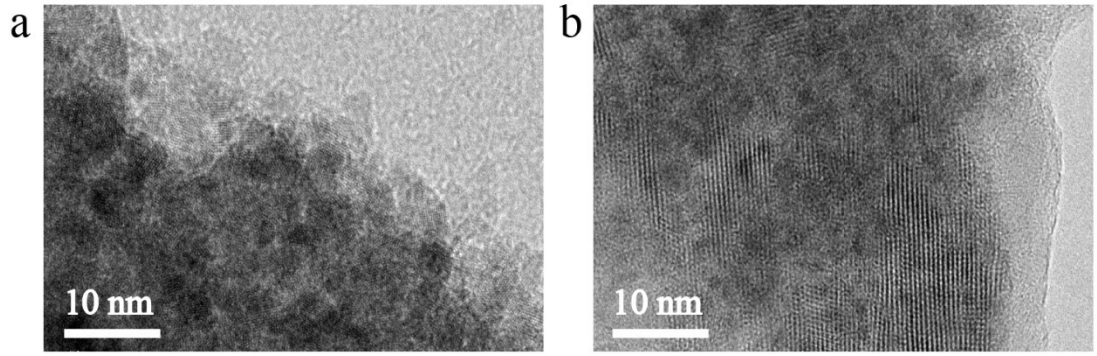

Fig. S9 High resolution transmission electron microscopy (HRTEM) images of the electrode powders after 100 cycles (a) $LiCoO_2$, (b) $LiCo_{0.98}Sb_{0.02}O_2$.

Table S1. The size distribution of bare and Sb doped $LiCoO_2$ determined by laser particle size analyzer. The particle size of Sb doped samples (the diameter at which 50% of a sample's mass comprises smaller particles (D50:~11μm) is smaller than that of bare $LiCoO_2$ (D50:~18μm).

Sample	Size distribution	
	D10(μm)	D50(μm)
$LiCoO_2$	8.58	18.01
$LiCo_{0.995}Sb_{0.005}O_2$	6.23	12.96
$LiCo_{0.99}Sb_{0.01}O_2$	5.78	11.23
$LiCo_{0.985}Sb_{0.015}O_2$	5.31	9.89
$LiCo_{0.98}Sb_{0.02}O_2$	5.44	10.38

Table S2. Comparison of the Co^{3+}/Co^{4+} redox peak difference in the cyclic voltammogram curves of bare $LiCoO_2$ and Sb doped $LiCoO_2$.

Sample	oxidation peak	reduction peak	ΔV (V)
$LiCoO_2$	4.00	3.86	0.14
$LiCo_{0.995}Sb_{0.005}O_2$	3.98	3.88	0.10

$LiCo_{0.99}Sb_{0.01}O_2$	3.98	3.88	0.10
$LiCo_{0.985}Sb_{0.015}O_2$	3.98	3.87	0.11
$LiCo_{0.98}Sb_{0.02}O_2$	3.98	3.88	0.10

Table S3. Summary of the electrochemical performances of $LiCoO_2$|Li half-cell reported in the literature.

Modified elements and method	Content	Voltage (V)	Rate	Residual capacity (mAh g^{-1})	Ref.
$LiAlSiO_4$ coating	2wt%	2.75-4.55	8C 1C=200 mA g^{-1}	160	8
Mn doping	5%	3.0-4.6	5C 1C=185 mA g^{-1}	135	9
Na doping	3%	3.0-4.3	10C 1C=140 mA g^{-1}	92	10
Zr doping	1%	3.0-4.3	10C 1C=140 mA g^{-1}	109	10
Nb doping	1%	3.0-4.3	10C 1C=140 mA g^{-1}	119	10
Al-doping and Li_2TiO_3-coating	1%	3.0-4.5	10C 1C=200 mA g^{-1}	128.6	11
Nanodot BaTiO3	<5%	3.3–4.2 V	100C 1C=160 mA g^{-1}	60	12
Mg doping	5%	3.0-4.6	4C 1C=270 mA g^{-1}	138	13
Sb	2%	3.0-4.5	100C 1C=220mA g^{-1}	93	This work

Table S4. Detailed computational conditions of $LiCoO_2$ and Sb-doped $LiCoO_2$ in delithiation process.

	a	b	b	α	β	γ	V	Volume change ratio
$LiCoO_2$	11.30	11.30	13.82				1529.26	
$LiCoO_2$-25	11.27	11.29	13.99	90.00	89.71	120.07	1540.36	0.73%
$LiCoO_2$-50	11.24	11.28	14.02	90.00	90.00	120.12	1538.08	0.58%
$LiCoO_2$-75	11.23	11.26	13.75	90.00	89.75	120.08	1504.62	-1.61%
	0.68%	0.43%	0.51%				-1.61%	
$LiCoSbO_2$	11.36	11.36	13.79				1540.97	
$LiCoSbO_2$-25	11.29	11.31	14.04	90.00	89.26	120.04	1551.96	0.71%
$LiCoSbO_2$-50	11.26	11.32	14.02	90.00	89.86	120.18	1546.95	0.39%
$LiCoSbO_2$-75	11.26	11.29	13.88	90.00	90.35	120.07	1528.27	-0.82%
	0.83%	0.63%	0.65%					

Notes and references

1. G. Kresse and J. Furthmuller, *Phys. Rev. B*, 1996, **54**, 11169-11186.
2. J. P. Perdew, K. Burke and M. Ernzerhof, *Phys. Rev. Lett.*, 1996, **77**, 3865-3868.
3. J. P. Perdew, M. Ernzerhof and K. Burke, *J. Chem. Phys.*, 1996, **105**, 9982-9985.
4. S. Grimme, Wires. Comput. *Mol. Sci.*, 2011, **1**, 211-228.
5. S. Grimme, *J. Comput. Chem.*, 2004, **25**, 1463-1473.
6. E. R. Johnson and A. D. Becke, *J. Chem. Phys.*, 2006, **124**, 174104.
7. P. E. Blöchl, *Phys. Rev. B*, 1994, **50**, 17953-17979.
8. B. Shen, X. Xu, W. Liu, M. Qin and W. Wang, *ACS Appl. Energy Mater.*, 2021, **4**, 12917-12926.
9. Y. T. Wang, T. Cheng, Z. E. Yu, Y. C. Lyu and B. K. Guo, *J. Alloys Compd.*, 2020, **842**, 155827.
10. K. Wu, Q. Li, M. Chen, D. Chen, M. Wu, Z. Hu, F. Li and X. Xiao, *J. Solid State Electrochem.*, 2018, **22**, 3725-3734.
11. Z. Cui, Z. Wang, Y. Zhai, R. Gao, Z. Hu and X. Liu, *J. Nanosci. Nanotechnol.*, 2020, **20**, 2473-2481.
12. S. Yasuhara, S. Yasui, T. Teranishi, K. Chajima, Y. Yoshikawa, Y. Majima, T. Taniyama and M. Itoh, *Nano Lett.*, 2019, **19**, 1688-1694.
13. Y. Y. Huang, Y. C. Zhu, H. Y. Fu, M. Y. Ou, C. C. Hu, S. J. Yu, Z. W. Hu, C. T. Chen, G. Jiang, H. K. Gu, H. Lin, W. Luo and Y. H. Huang, *Angew Chem. Int. Edit.*, 2021, **60**, 4682-4688.